Polymer 49 (2008) 4871–4876

Contents lists available at ScienceDirect

Polymer

journal homepage: www.elsevier.com/locate/polymer

Carboxylated butadiene–styrene rubber/halloysite nanotube nanocomposites: Interfacial interaction and performance

Mingliang Du, Baochun Guo*, Yanda Lei, Mingxian Liu, Demin Jia

Department of Polymer Materials and Engineering, South China University of Technology, Guangzhou 510640, China

ARTICLE INFO

Article history:
Received 1 May 2008
Received in revised form 16 July 2008
Accepted 28 August 2008
Available online 3 September 2008

Keywords:
Carboxylated styrene–butadiene rubber
Halloysite nanotubes
Hydrogen bonding

ABSTRACT

A co-coagulation process was utilized to prepare carboxylated butadiene–styrene rubber (xSBR)/halloysite nanotube (HNT) nanocomposites. The interfacial interaction, morphology, and the mechanical performance of the nanocomposites were investigated. Attenuated total reflection Fourier transform infrared spectroscopy (ATR-FTIR) and X-ray photoelectron spectroscopy (XPS) results indicate the formation of hydrogen bonding between xSBR and HNTs. Lower content of HNTs tends to delay the vulcanization of xSBR/HNT compounds, while higher HNT loading promotes the vulcanization. It is shown that HNTs are dispersed individually and uniformly in the matrix with strong interfacial bonding. The mechanical properties, especially the modulus and hardness, are significantly increased by the inclusion of HNTs. The significant reinforcing effects of HNTs are correlated to the co-coagulation process and strong interfacial interactions via hydrogen bonding.

1. Introduction

Polymer nanocomposites incorporated with inorganics have drawn much attention during past decade due to their unprecedented performance compared with the conventional polymer composites [1–3]. It is generally believed that the interfacial interactions are important in determining the final performance of polymer nanocomposites incorporated with inorganics. The interfacial interactions between polymer matrix and inorganics mainly include van der Waals force, hydrogen bonds, covalent bonds and ionic bonds [4–7]. Many approaches have been developed to improve the interfacial interactions of the nanocomposites, including the modification of inorganics [8–10] or matrix [11]. So far, new effective approaches to improve the interfacial interaction of nanocomposites are still being focused.

Recently, halloysite nanotubes (HNTs), a type of naturally occurring silicates with nanotubular structures were disclosed to reinforce polymers and unique reinforcing effects to different polymers such as epoxy resin, polypropylene, polyamide, natural rubber, etc. have been demonstrated [12–15]. As reported [16,17], HNTs are aluminosilicates with predominantly tubular structure at nanoscale and the surface of HNTs is composed of siloxane and has only a few hydroxyl groups, which indicates that HNTs possess much better dispersion property than other natural silicates such as montmorillonite and kaolinite and potential ability for the formation of hydrogen bonding. xSBR is a copolymer of styrene, butadiene and a small amount of acrylic acid and it is expected the carboxyl groups introduced by acrylic acid are also potential functionality for the formation of hydrogen bonding. Actually, tailoring the structures and performance of the polymer blends or composites through the formation of hydrogen bonding in the systems have been widely reported [18–26]. In the present work, HNTs and xSBR are utilized to prepared nanocomposites with strong interfacial interactions via hydrogen bonding. The interfacial hydrogen bonding in xSBR/HNT nanocomposites was fully characterized and its effect on curing characteristics, morphology and the mechanical properties was investigated.

2. Experimental section

2.1. Materials

xSBR latex, with solid content of 50%, was manufactured by Guangzhou Juntai Materials Co. Ltd. The xSBR is a copolymer of styrene, butadiene, acrylic acid and the chemical structure of xSBR is shown below.

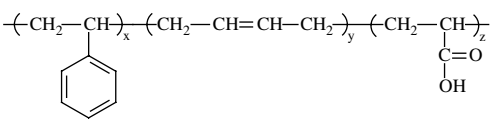

Chemical structure of xSBR (x/y/z=42.0/56.4/1.6)

The HNTs were mined from Hubei Province, China and purified according to the reported procedure [15]. The Brunauer–Emmett–Teller (BET) specific surface area was determined as 50.45 m^2/g.

* Corresponding author. Tel.: +86 20 87113374; fax: +86 20 22236688.
E-mail address: psbcguo@scut.edu.cn (B. Guo).

0032-3861/$ – see front matter © 2008 Elsevier Ltd. All rights reserved.
doi:10.1016/j.polymer.2008.08.042

Table 1
Composition of xSBR/HNT nanocomposites[a]

Sample code	xSBR	xSBR2H	xSBR5H	xSBR10H	xSBR20H	xSBR30H
xSBR	100	100	100	100	100	100
HNTs	0	2	5	10	20	30

[a] Rubber intergradient: zinc oxide, 5 phr; stearic acid, 1 phr; 2-mercapto benzothiazole (M), 0.1 phr; dibenzothiazole disulfide (DM), 1.3 phr; diphenyl guanidine (DPG), 0.3 phr; tetramethyl-thiuram monosulfide (TS), 0.2 phr; *N*-isopropyl-*N*′-phenyl-*p*-phenylenediamine (4010NA), 1.5 phr; sulphur (S), 1.5 phr.

Sulphur, zinc oxide, stearic acid, accelerators, and other additives were of industrial grade and used as-received.

2.2. Preparation of xSBR/HNT nanocomposites

HNTs aqueous suspension (10 wt.%) and xSBR latex were mixed and stirred for 30 min. Then the mixture was co-coagulated by adding calcium chloride aqueous solution (1 wt.%). The co-coagulated compound was washed with de-ionized water for several times until no chlorine ion was detected. Then the compound was vacuum dried at 80 °C for 5 h. The dried compound was compounded with rubber additives with a two-roll mill and then compression molded at 150 °C. The composition of xSBR/HNT nanocomposites is tabulated in Table 1.

2.3. Characterizations

2.3.1. Determination of specific surface area and pore width distribution

To characterize the absorbing ability of HNTs toward rubber accelerators, a model compound of HNTs/DM (weight ratio of 30/2) was prepared by vigorously mixing the components at 10 000 rpm for 3 min. The Brunauer–Emmett–Teller (BET) specific surface area and the Barrett–Joyner–Halenda (BJH) pore width distribution were determined with specific surface area and porosity analyzer, ASAP 2020 of Micromeritics.

2.3.2. Attenuated total reflection Fourier transform infrared spectroscopy (ATR-FTIR) and X-ray photoelectron spectroscopy (XPS)

To characterize the possible interactions between xSBR and HNTs, the co-coagulated xSBR/HNT compounds (weight ration of 50/50) without any other additives were processed with a two-roll mill into a thin sheet for ATR-FTIR analysis. The ATR-FTIR analysis was conducted by a Bruker Vector 33 spectrometer. Spectra were taken from 4000 cm^{-1} to 400 cm^{-1}. XPS spectra of HNTs and xSBR/HNT compounds were recorded by using an X-ray photoelectron spectrometer (Kratos Axis Ultra DLD) with an Aluminum (mono) Kα source (1486.6 eV). The Aluminum Kα source was operated at 15 kV and 10 mA. For all the samples, a high-resolution survey (pass energy = 48 eV) was performed at spectral regions relating to silicon and aluminum atoms.

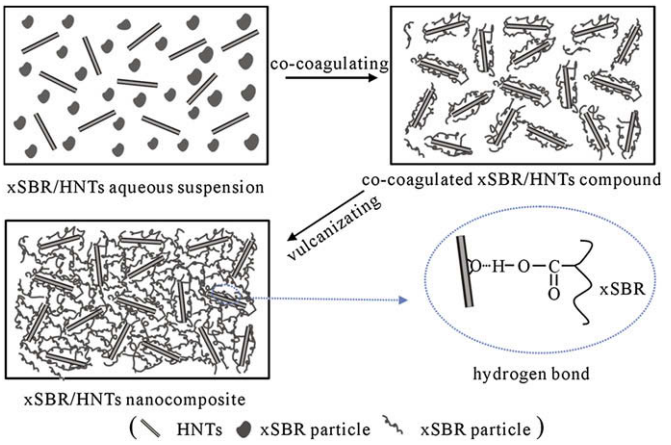

Fig. 1. Scheme of preparation process of xSBR/HNT nanocomposites.

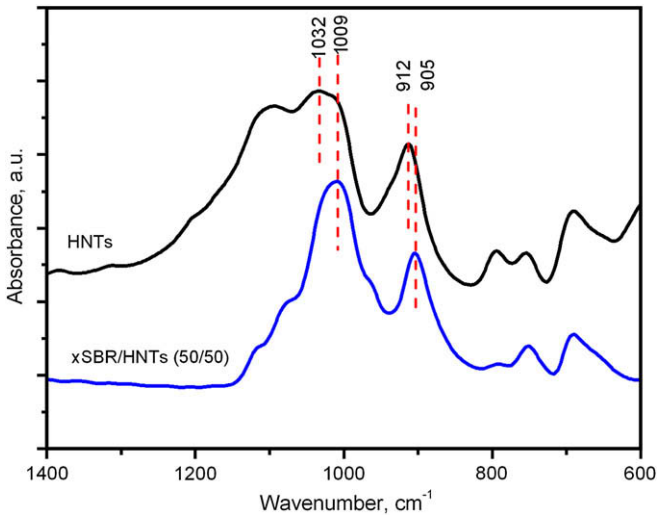

Fig. 2. ATR-FTIR spectra of HNTs and xSBR/HNT compounds.

2.3.3. Determination of curing characteristics

The curing characteristics of the xSBR compound were determined at 150 °C by a U-CAN UR-2030 vulcameter, Taiwan.

2.3.4. Scanning electron microscopy (SEM)

The fracture surfaces of tensile samples were plated with a thin layer of gold before any observations. The SEM observations were then performed using a Philips KL 30 SEM machine.

2.3.5. Transmission electron microscopy (TEM)

The specimens of vulcanizates were ultramicrotomed into thin pieces of about 120 nm in thickness with Leica EM UC6. Then the TEM observations were done using a Hitachi H-7500 electron transmission microscope machine at an accelerating voltage of 30 kV.

2.3.6. Mechanical performance

Tensile tests were performed following ISO standard 37-2005 at 25 °C. Tensile strength, modulus and elongation at break were measured using U-CAN UT-2060 (Taiwan) instrument. Shore A hardness was performed following ISO standard 7619-1986 using an XY-1 sclerometer (Shanghai).

3. Results and discussion

3.1. Interfacial interaction between xSBR and HNTs

In order to obtain well dispersion of HNTs in xSBR, a co-coagulation process of xSBR latex and HNT aqueous solution was

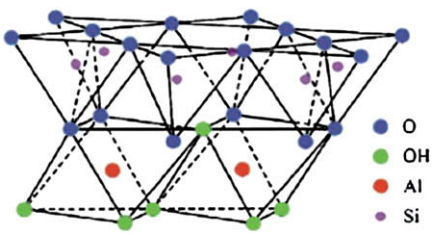

Fig. 3. Crystalline structure of HNTs.

utilized and the process is depicted in Fig. 1. In the process, with the addition of co-coagulation agent into the xSBR/HNT aqueous suspension, the emulsified particles of xSBR coagulated promptly and consequently the HNTs among the particles were embedded in the coagulated xSBR. The co-coagulation process effectively prevents HNTs from aggregation and ensures the uniform dispersion of HNTs in xSBR matrix.

FTIR technique is often utilized to characterize the formation of hydrogen bonding [27–31]. Fig. 2 shows the ATR-FTIR spectra of HNTs and xSBR/HNT compounds. The absorption around 1030 cm^{-1} and 914 cm^{-1} is assigned to the absorptions of Si–O stretching vibrations and Al–OH librations in HNTs respectively. However, for the FTIR spectra of xSBR/HNT compound, there's a blue shift of about 21 cm^{-1} for the absorption of Si–O stretching vibrations, whereas the blue shift of the absorption of Al–OH librations is only about 7 cm^{-1}. Typical crystalline unit of HNTs, as shown in Fig. 3, consists of two-layer structure and contains two types of hydroxyl groups, outer hydroxyl groups and inner hydroxyl groups, which are situated in the unshared plane of tetrahedral sheet (silicon and oxygen) and shared octahedral sheet (aluminum and oxygen) respectively. As a consequence, the outer side of HNTs is siloxane and only a few of Si–OH groups are located in HNT ends and surface defects. However, most of Al–OH groups are situated in the inner side. It is believed that the formation of hydrogen bonding

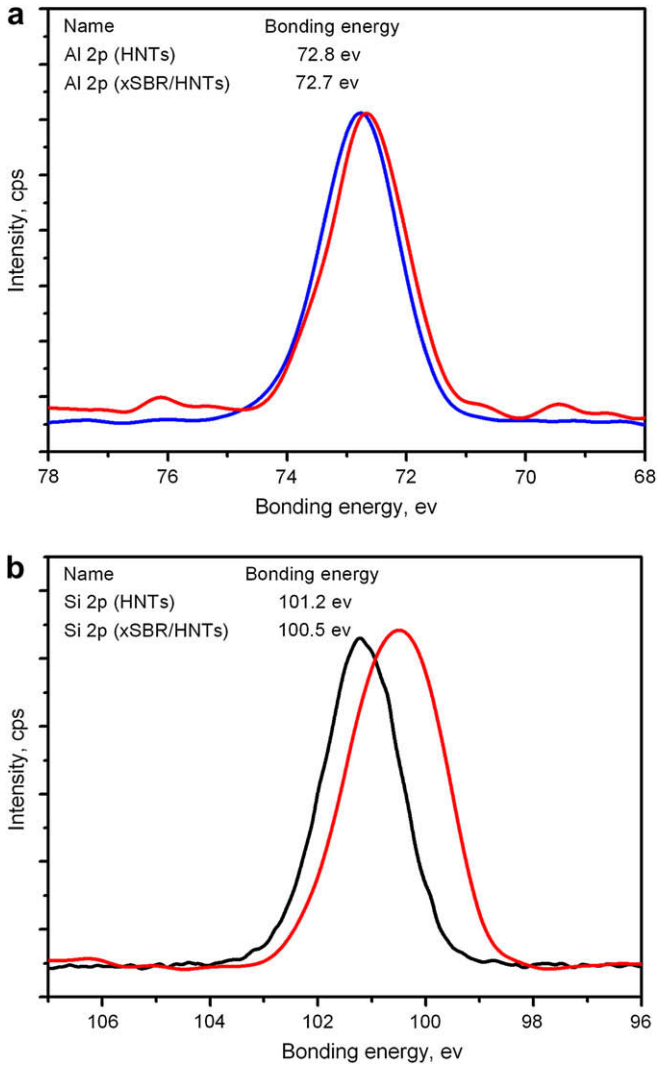

Fig. 4. High-resolution XPS spectra of silicon and aluminum in HNTs and xSBR/HNT compound (50/50).

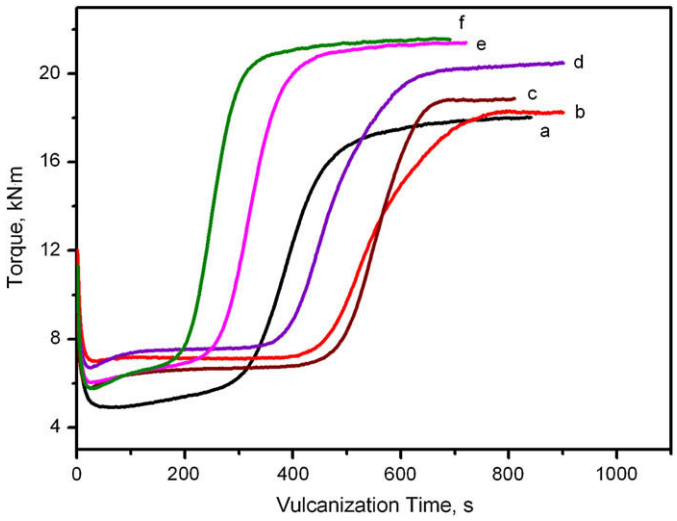

Fig. 5. Curing behavior of xSBR/HNT compounds.

results in the blue shift of the FTIR absorption of Si–O stretching. Because most of the Al–OH groups are situated in the inner side of the crystalline structure as described above, the blue shift for the absorption of aluminols is much smaller than that for the Si–O.

XPS survey was performed in order to further substantiate the formation of hydrogen bonding between HNTs and xSBR. It is believed that the formation of hydrogen bonding will lead to the variation of the chemical environment for the hydrogen bonding functionalities, which can be characterized by the variation of bonding energy of the atoms related to the hydrogen bonding via XPS survey [32–34]. Fig. 4 shows the high-resolution XPS spectra of silicon and aluminum atoms in HNTs and xSBR/HNT compound respectively. As shown in Fig. 4, there's some decrease in the bonding energy of silicon atom and aluminum atoms, which are connected to the oxygen atom in the hydrogen bond. One can see that the decreases in bonding energy for silicon and aluminum are 0.7 eV and 0.1 eV respectively. The more significant decrease for the bonding energy of silicon atoms is ascribed to the fact that most of the hydrogen bonds in the system are formed between Si–O and carboxyl groups of xSBR. As discussed above, most of Al–OH groups are situated in the inner side and consequently it is much difficult to participate in the formation of hydrogen bonding between Al–OH and carboxyl groups of xSBR. Consequently, the bonding energy variation of silicon atoms is much obvious than that of aluminum atoms. This further confirms the formation of hydrogen bonding in the xSBR/HNT compound.

3.2. Curing characteristics of the xSBR/HNT compounds

Generally, as reported by many other literatures [35–37], incorporation of silicates in rubber matrix delays the vulcanization of rubber matrix, which usually is ascribed to the adsorption

Table 2
Curing characteristics of xSBR/HNT compounds

Compound codes	Scorch time (T_{c10}), s	Curing time (T_{c90}), s	Equilibrium torque, kN m
xSBR	296	583	18.0
xSBR2H	464	680	18.3
xSBR5H	458	624	18.9
xSBR10H	374	589	20.5
xSBR20H	249	396	21.4
xSBR30H	190	311	21.6

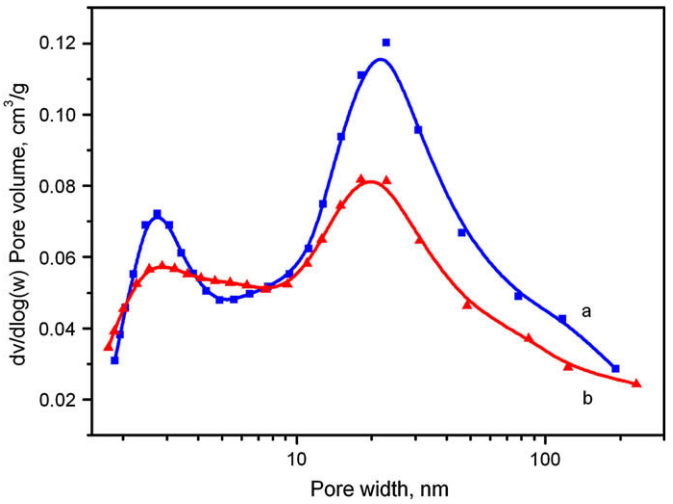

Fig. 6. BJH pore volume distribution curve of HNTs (a) and HNTs/DM mixture (30/2) (b).

between silicates and vulcanization additives such as accelerators. However, as shown in Fig. 5, when incorporating HNTs, xSBR exhibits exceptional vulcanization behavior. Lower content of HNTs tends to delay the vulcanization of xSBR/HNT compounds, while higher HNT loading promotes the vulcanization. The characteristics of the vulcanization of xSBR and xSBR/HNT compounds are summarized in Table 2. As indicated in Table 2, with the inclusion of 2 phr of HNTs, both the scorch time and optimum curing time are increased substantially. However, with the increase of inclusion of HNTs, the vulcanization of xSBR/HNT compounds is promoted significantly. Generally, natural silicate is a class of mesoporous materials, which tend to absorb organics via different mechanism such as acid–base interaction, hydrogen bonding or charge transfer, etc. [38–40]. The delayed vulcanization of rubber by silicate such as kaolinite and montmorillonite has been widely reported. HNTs belong to kaolinite class, their absorbing ability toward a number of chemicals has also been studied [41]. To verify the adsorption capacity of accelerator such as DM by HNTs, the determination of BJH pore distribution of HNTs and HNTs/DM mixture was conducted and the results are shown in Fig. 6. For HNTs, the pore width around 2 nm and 25 nm is assigned as the mesopores due to the surface defects, and inner diameter of the tubes respectively. However, for the HNTs/DM mixture, in which a certain amount of DM was absorbed onto the surface of HNTs during vigorously mixing, the two peaks are decreased obviously, suggesting the adsorption of DM on the surface and in the lumen of HNTs. Consequently, it is believed that the delayed vulcanization of the compounds with lower content of HNTs is attributed to the adsorption of accelerators on the surface and in the lumen of HNTs.

Apart from the adsorption effects, it is believed that another mechanism influences the vulcanization of the nanocomposites, which is illustrated in Fig. 7. As shown, the hydrogen bonds between Si–O on HNTs and carboxyl groups on xSBR chain actually act as efficient crosslinks in the vulcanizates. More HNTs present,

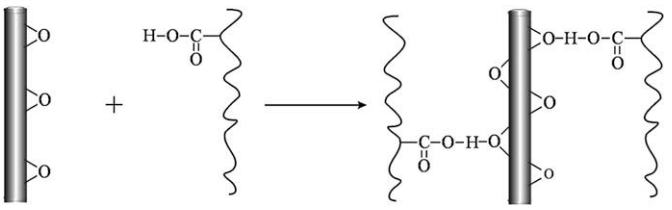

Fig. 7. Physical crosslink via hydrogen bonding between xSBR and HNTs.

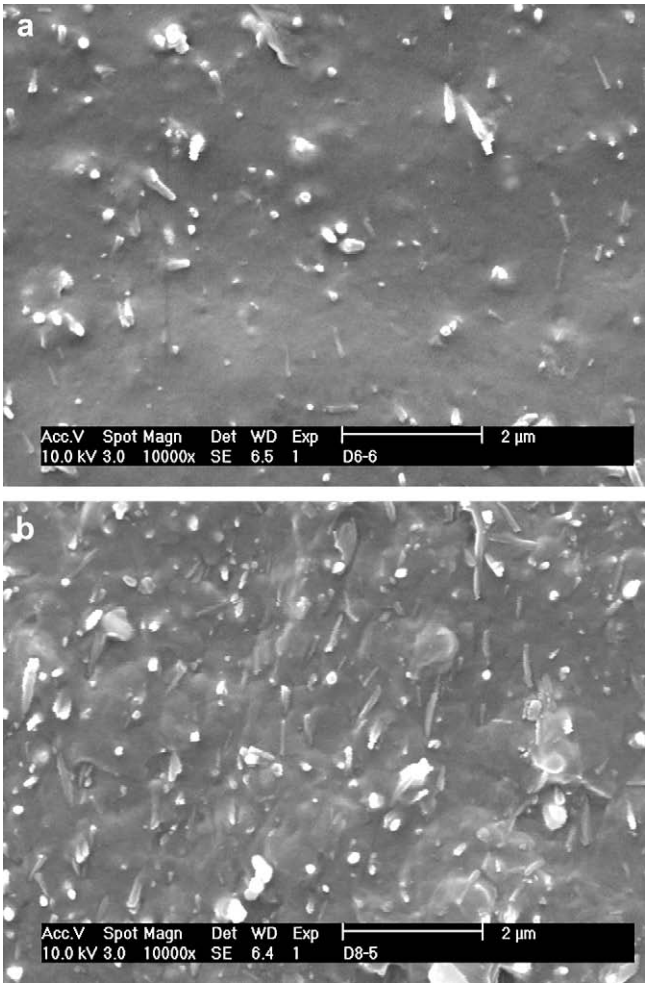

Fig. 8. SEM photos of xSBR/HNT nanocomposites a) xSBR5H; b) xSBR20H.

more hydrogen bonds (crosslinks) result. This effect tends to accelerate the vulcanization of the nanocomposites. When the HNT content is relatively low, the effect of adsorption of the accelerators onto the surface of HNTs plays the leading role, resulting in delayed curing behavior. However, when the HNT content is high enough, the effect of the formation of hydrogen bonds (crosslinks) dominates, resulting in accelerated vulcanization. Although the equilibrium torque of the compound during curing shows slightly increasing trend, the formation of hydrogen bonding in the nanocomposites has significant effects on the mechanical performance of the nanocomposites, which will be discussed below.

3.3. Morphology of SBR/HNT nanocomposites

Fig. 8 shows the SEM photos of the tensile fractured surface of the xSBR nanocomposites. It is shown that HNTs with tubular structure are uniformly dispersed in the matrix. In addition, the interface between HNTs and rubber matrix is blurry and nearly no debonded HNTs and cavities are observed in the fractured surface of the nanocomposites, suggesting the very strong interfacial bonding between HNTs and xSBR matrix. The revealed strong interfacial bonding is attributed to the presence of the interfacial hydrogen bonds between HNTs and rubber matrix.

Fig. 9 shows the TEM photos of nanocomposites with 5 phr and 20 phr HNT loading. The TEM photos of the nanocomposites suggest that HNTs are dispersed uniformly and individually in xSBR matrix, which is attributed to the virtue of the co-coagulation process and the hydrogen bonding between HNTs and xSBR matrix.

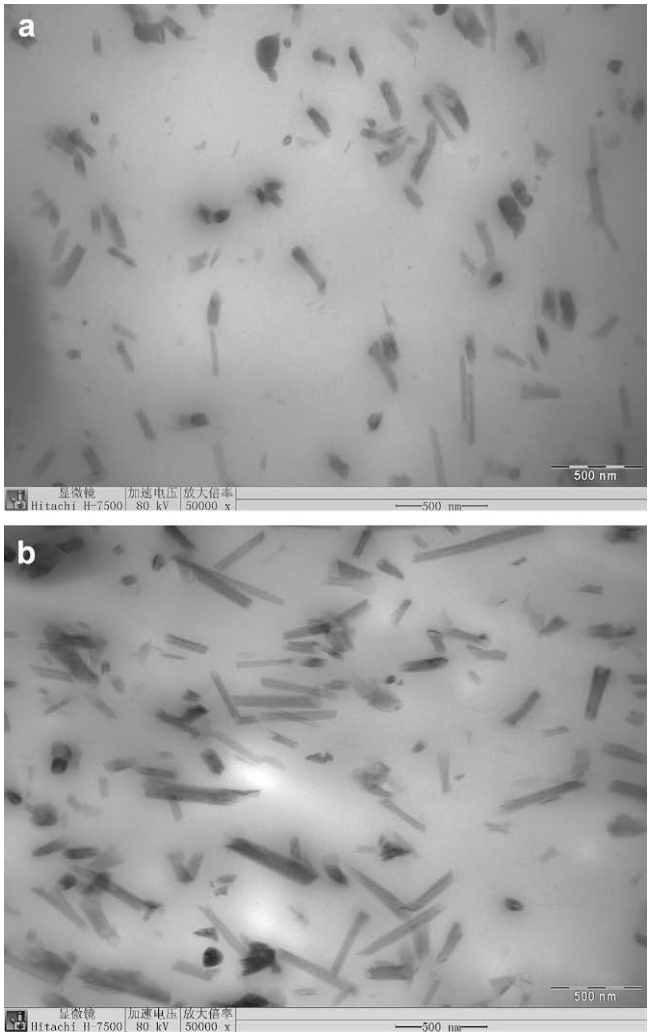

Fig. 9. TEM photos of xSBR/HNT nanocomposites a): xSBR5H; b): xSBR20H.

3.4. Mechanical performance

The tensile stress–strain curves of the xSBR/HNT nanocomposites are shown in Fig. 10. The mechanical properties of the nanocomposites are tabulated in Table 3. As shown in Fig. 10, not only the ultimate stress increases with HNT loading, but also the modulus of the nanocomposites increases significantly with HNT loading. It can be seen from Table 3 that with the inclusion of only 5 phr of HNTs, the modulus at 100% elongation is almost doubled compared with that of neat xSBR vulcanizate. With further increase of HNT loading, the modulus of xSBR/HNT nanocomposites increases consistently. Because of inherently high cohesive energy of xSBR due to the presence of intermolecular hydrogen bonding, the neat xSBR vulcanizate shows much higher tensile and tear strength and lower elongation at break compared with those for the general purpose SBR. Still, the incorporation of HNTs tends to further increase the tensile and tear strength. Noticeably, the hardness of xSBR/HNT nanocomposites also surprisingly increased with HNT loading. Incorporations of 2 phr and 5 phr HNTs lead to increment of 7 and 15 degree in hardness respectively. This increment is quite remarkable. Generally, 3–4 phr silicate or carbon black is needed to obtain 1 degree increment in hardness [42–45]. As described above, inclusion of small amount of HNTs may increase the physical crosslinking density via hydrogen bonding, consequently the hardness of the vulcanizates is steeply increased with HNT loading. It is believed that the above significant reinforcing effects of HNTs are attributed to uniformly dispersed nanotubes with high *L*/*D* ratio and strong interfacial interaction due to the hydrogen bonding between the nanotubes and the matrix.

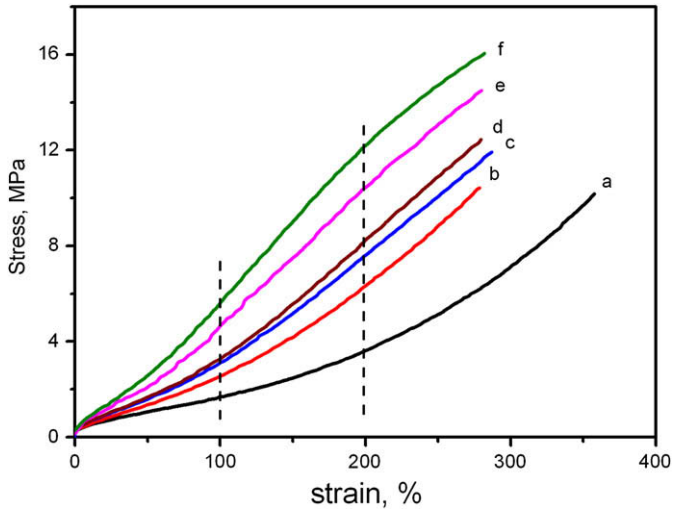

Fig. 10. Stress–strain curve of xSBR and xSBR/HNT nanocomposites a) xSBR; b) xSBR2H; c) xSBR5H; d) xSBR10H; e) xSBR20H; f) xSBR30H.

Table 3
Mechanical properties of xSBR/HNT nanocomposites (Data in the parenthesis is the standard variation)

Nanocomposites	Modulus at 100% elongation, MPa	Tensile strength, MPa	Tear strength, kN/m^2	Elongation at break, %	Hardness, Shore A
xSBR	1.52 (0.16)	10.0 (0.44)	19.4 (1.63)	372 (20.0)	55
xSBR2H	2.37 (0.22)	10.4 (0.52)	25.2 (1.25)	236 (18.2)	62
xSBR5H	2.92 (0.30)	11.4 (0.58)	26.0 (0.31)	277 (19.2)	70
xSBR10H	3.48 (0.20)	12.9 (0.09)	32.0 (1.84)	279 (22.2)	75
xSBR20H	5.08 (0.21)	13.6 (0.62)	36.0 (2.15)	259 (21.3)	78
xSBR30H	5.56 (0.19)	15.3 (0.77)	32.0 (0.92)	267 (17.3)	80

4. Conclusion

Carboxylated butadiene–styrene rubber (xSBR)/halloysite nanotube (HNT) nanocomposites with individually dispersed HNTs and strong interfacial bonding were prepared by co-coagulation method. Strong hydrogen bonding was formed in the nanocomposites. Inclusion of lower content of HNTs delayed the vulcanization of xSBR/HNT compounds, while higher HNT loading accelerated the vulcanization. The mechanical properties, especially the modulus and hardness, were significantly enhanced by the incorporation of HNTs. The significant reinforcing effects of HNTs were correlated to the co-coagulation process and strong interfacial interactions via hydrogen bonding.

Acknowledgements

We are grateful for the financial support by the National Natural Science Foundation of China with grant number of 50603005.

References

[1] Alexandre M, Dubois P. Mater Sci Eng R 2000;28(1–2):1–63.
[2] Cho JW, Paul DR. Polymer 2001;42(3):1083–94.
[3] Shi ZQ, Gao XP, Song DY, Zhou YF, Yan DY. Polymer 2007;48(26):7516–22.
[4] Laine RM, Choi JW, Lee I. Adv Mater 2001;13(11):800–3.
[5] Rong MZ, Zhang MQ, Pan SL, Lehmann B, Friedrich K. Polym Int 2004;53(2):176–83.

[6] Kelnar I, Khunova V, Kotek J, Kapralkova L. Polymer 2007;48(18):5332–9.
[7] Lim JS, Noda I, Im SS. Polymer 2007;48(9):2745–54.
[8] Pramanik N, Mohapatra S, Alam S, Pramanik P. Polym Compos 2008;29(4):429–36.
[9] Yan SF, Yin JB, Yang Y, Dai ZZ, Ma J, Chen XS. Polymer 2007;48(6):1688–94.
[10] Isoda K, Kuroda K, Ogawa M. Chem Mater 2000;12(6):1702–7.
[11] Motha K, Hippi U, Hakala K, Peltonen M, Ojanpera V, Lofgren B, et al. J Appl Polym Sci 2004;94(3):1094–100.
[12] Liu MX, Guo BC, Du ML, Cai XJ, Jia DM. Nanotechnology 2007;18:455703.
[13] Du ML, Guo BC, Liu MX, Jia DM. Polym J 2006;38(11):1198–204.
[14] Guo BC, Zou QL, Lei YD, Du ML, Liu MX, Jia DM. New Chem Mater (in Chinese) 2008;36(6):32–4.
[15] Liu L, Jia ZX, Guo BC, Liu MX, Du ML, Jia DM. Rubber Ind (in Chinese) 2008;55(3):133–7.
[16] Joussein E, Petit S, Churchman J, Theng B, Righi D, Delvaux B. Clay Miner 2005;40(4):383–426.
[17] Ye YP, Chen HB, Wu JS, Ye L. Polymer 2007;48(21):6426–33.
[18] Ohgi H, Yang H, Sato T, Horii F. Polymer 2007;48(13):3850–7.
[19] Collins G, Yoo SU, Recber A, Jaffe M. Polymer 2007;48(4):975–88.
[20] Wang LF. Polymer 2007;48(3):894–900.
[21] Kim J, Sandoval RW, Dettmer CM, Nguyen ST, Torkelson JM. Polymer 2008;49(11):2686–97.
[22] Hameed N, Guo QP. Polymer 2008;49(4):922–33.
[23] Das S, Yilgor I, Yilgor E, Wilkes GL. Polymer 2008;49(1):174–9.
[24] Araki J, Ito K. Polymer 2007;48(24):7139–44.
[25] Liu QT, Zhang H, Yin SY, Wu LX, Shao C, Su ZM. Polymer 2007;48(13):3759–70.
[26] Krakovsky I, Hanykova L, Trchova M, Baldrian J, Wubbenhorst M. Polymer 2007;48(7):2079–86.
[27] Kotrel S, Lunsford JH, Knozinger H. J Phys Chem B 2001;105(18):3917–21.
[28] Pei KM, Li YM, Li HY. J Mol Struct 2003;660:113–8.
[29] Shieh YT, Liu KH. J Supercrit Fluids 2003;25(3):261–8.
[30] Ma G, Allen HC. J Phys Chem B 2003;107(26):6343–9.
[31] Uno B, Okumura N, Goto M, Kano K. J Org Chem 2000;65(5):1448–55.
[32] Li L, Chan CM, Weng LT, Xiang ML, Jiang M. Macromolecules 1998;21:7248–55.
[33] Li L, Chan CM, Weng LT. Polymer 1998;39(11):2355–60.
[34] Liu SY, Chan CM, Weng LT, Jiang M. J Polym Sci Part B 2005;43:1924–30.
[35] Kim MS, Kim GH, Chowdhury SR. Polym Eng Sci 2007;47(3):308–13.
[36] Ramier J, Chazeau L, Gauthier C, Guy L, Bouchereau MN. Rubber Chem Technol 2007;80(1):183–93.
[37] Choi D, Kader MA, Cho BH, Huh Y, Nah C. J Appl Polym Sci 2005;98(4):1688–96.
[38] Choi SS, Nah C, Byung-Wook J. Polym Int 2003;52:1382–9.
[39] Kosmalska A, Zaborski M, Slusarski L. Macromol Symp 2003;194:269–75.
[40] Lopez-Manchado MA, Arroyo M, Herrero B, Biagiotti J. J Appl Polym Sci 2003;89:1–15.
[41] Theng BKG. The chemistry of clay–organic reactions. London: Adam Hilger; 1974.
[42] Arroyo M, Lopez-Manchado MA, Herrero B. Polymer 2003;44(8):2447–53.
[43] Wang YZ, Zhang LQ, Tang CH, Yu DS. J Appl Polym Sci 2000;78(11):1879–83.
[44] Varghese S, Karger-Kocsis J. Polymer 2003;44(7):4921–7.
[45] Ganter M, Gronski W, Reichert P, Mulhaupt R. Rubber Chem Technol 2001;74(2):221–35.